Nonperturbative calculations of double photoionization of Ne: An *R* matrix with pseudostate-convergence study

D. C. Griffin
Department of Physics, Rollins College, Winter Park, Florida 32789, USA

C. P. Ballance and M. S. Pindzola
Department of Physics, Auburn University, Auburn, Alabama 36849, USA

(Received 13 April 2009; revised manuscript received 9 July 2009; published 25 August 2009)

The *R* matrix with pseudostate (RMPS) method has been employed to perform nonperturbative calculations of the total cross sections for single-photon double photoionization of ground-state Ne. A series of calculations was performed in which the number of pseudostates included in the close-coupling expansion was varied. Within the constraints of currently available massively parallel computers, we were able to achieve reasonably good convergence of the double photoionization cross section for Ne. The final RMPS results in both the length and the velocity gauges are compared to double photoionization cross sections determined from many-body perturbation-theory calculations and synchrotron measurements.

DOI: 10.1103/PhysRevA.80.023420 PACS number(s): 32.80.Fb

I. INTRODUCTION

Single-photon double photoionization is a prime example of quantal three-body problems, which continue to present a significant challenge to atomic scattering theory, especially for complex atomic targets. Nonperturbative methods such as convergent close coupling (CCC), time-dependent close coupling (TDCC), *R* matrix with pseudostates (RMPS), and hyperspherical close coupling have been successfully applied to the calculation of single-photon double photoionization of He [1–8]. In addition, the CCC and the TDCC methods have been applied to double photoionization of ground-state Be [9–11] and the CCC method to ground-state Mg and Ca [12]. Recently, we employed the RMPS method to determine the total double photoionization of ground and metastable Be and Mg and the TDCC method to calculate double photoionization of ground-term Mg [13].

The RMPS method, in which the second electron ejected from the target is represented by a large set of L_2 pseudostates, has proven ideally suited to the calculation of total double photoionization of alkaline-earth metals such as Be and Mg, where the final ion is left in a closed shell. However, its application to an inert-gas atom such as Ne presents much greater difficulties; this is solely because the final ion is in either the $2s^2 2p^4$ or the $2s2p^5$ open-shell configuration (the closed-subshell $2p^6$ configuration is also possible, but the cross section for double photoionization of the $2s^2$ subshell is quite small). First of all, this requires a very large close-coupling (CC) expansion for the *N*-electron singly ionized species that includes the Rydberg series: $2s^2 2p^4(^1S)nl$, $2s^2 2p^4(^3P)nl$, $2s^2 2p^4(^1D)nl$, $2s2p^5(^3P)nl$, and $2s2p^5(^1P)nl$. However, with recent developments of highly efficient parallel *R*-matrix programs, which address the problem of calculating and storing large numbers of $(N+1)$-electron eigenvectors and bound-free dipole matrix elements, it is now possible to apply this method to such large expansions.

There is a second problem that cannot be overcome. For completeness in any *R*-matrix calculation employing an orthonormal set of bound-electron wave functions, one must include all possible $(N+1)$-electron bound terms that can be formed by adding one of the bound electrons to all the terms included in the *N*-electron CC expansion for the ion. This leads to a highly correlated $2s^2 2p^6\ ^1S$ ground term that includes all single-electron promotions out of the $2s$ and the $2p$ subshells and all two-electron promotions out of $2p$ as well as one out of $2s$ and one out of $2p$ through the highest value of n included in the CC expansion of the residual ion. However, to include the same amount of configuration-interaction (CI) in the terms within the expansion for the residual ion would render the calculation impossibly large. This is illustrated in Table I. The second column lists the configurations included in the CC expansion for the residual ion. The first column lists all the $(N+1)$-electron configurations of the target atom formed by adding one bound electron to the ion configurations, as described above. In the third column, the first two sets of configurations would be required to provide an equivalent amount of CI for the $2s^2 2p^5\ ^2P$ ground term of the residual ion as that included in the $2s^2 2p^6\ ^1S$ ground term of the target atom for the determination of the ionization energy of the target. The next three sets of configurations would be needed to provide a similar balance for the pseudostates used to describe the second electron ejected from the target in the determination of the double photoionization cross section. Clearly, the number of such configurations would be impossibly large, and this imbalance will affect both the calculated ionization energy of the target and the agreement between the length-gauge and the velocity-gauge double photoionization cross sections.

Although there are presently no published nonperturbative calculations of the single-photon double photoionization of Ne, many-body perturbation theory (MBPT) has been applied to this problem [14–18]. A primary uncertainty in such MBPT calculations is associated with the potential that should be employed to generate the basis set for the perturbative calculations; this problem is discussed extensively by Carter and Kelly [16]. Kilin *et al.* [17] demonstrated that there are very large differences between calculated double photoionization cross sections that employ a $V^{(N-1)}$ potential

TABLE I. An illustration of the imbalance between the large amounts of CI included in the initial target compared to the amounts of CI included in the residual ion.

Target atom configurations	Residual-ion configurations	Omitted residual-ion configurations
$2s^22p^6$	$2s^22p^5$	$2s^22p^3n'l'n''l''$
$2s^22p^5nl$	$2s2p^6$	$2s2p^4n'l'n''l''$
$2s2p^6nl$	$2s^22p^4nl$	$2s^22p^2nln'l'n''l''$
$2s^22p^4nln'l'$	$2s2p^5nl$	$2s2p^3nln'l'n''l''$
$2s2p^5nln'l'$		$2p^4nln'l'n''l''$

versus those that employ a $V^{(N-2)}$ potential. They then attempted to overcome this problem by employing a $V^{(N-q)}$ potential with a fractional charge q that was adjusted to minimize the difference between the length- and velocity-gauge cross sections [18].

Over a period of about 25 years, a large number of measurements of the double photoionization of Ne were performed using synchrotron radiation [19–25]. However, there is a significant spread among the various measurements that makes any definitive comparison of theory with experiment impossible.

The remainder of this paper is organized as follows: in Sec. II, we provide a description of the RMPS method and its application to the double photoionization of Ne; in Sec. III, we present double photoionization cross-section results for Ne; and in Sec. IV, we conclude with a brief summary.

II. THEORETICAL AND COMPUTATIONAL METHODS

The application of the R-matrix method to photoionization is described in detail by Burke and Taylor [26] and Berrington *et al.* [27] and is summarized by Griffin *et al.* [13]. In atomic units, the total cross section for photoionization in LS coupling is given in the dipole approximation by

$$\sigma = \frac{8\pi^2\alpha\omega}{3(2L_i+1)}\sum_{l_fL}|\langle\Psi_f^-\|\mathbf{D}\|\Psi_i\rangle|^2, \tag{1}$$

where ω is the photon energy, α is the fine structure constant, and the coefficient of the asymptotic form of the Coulomb functions is $(\pi k)^{-1/2}$. The dipole operator is given by

$$\mathbf{D} = \sum_{\mathbf{i=1}}^{\mathbf{N+1}} \mathbf{r_i} \tag{2}$$

in the length gauge and by

$$\mathbf{D} = \frac{1}{\omega}\sum_{\mathbf{i=1}}^{\mathbf{N+1}} \boldsymbol{\nabla}_\mathbf{i} \tag{3}$$

in the velocity gauge. Ψ_i is the initial $(N+1)$-electron bound target wave function with a total angular momentum L_i and Ψ_f^- is the final wave function with a total angular momentum L, for which the wave function of the ion with a total angular momentum L_f and a total spin S_f is coupled to a continuum-electron wave function of angular momentum l_f.

Within an inner region $r \le a$, where electron correlation and exchange are important, the $(N+1)$-electron wave functions Ψ_i and Ψ_f^- are expanded in terms of R-matrix basis functions. In the outer region $(r>a)$, the continuum wave functions are determined at each energy by solving CC equations without exchange; they are then matched to the solutions in the inner region at $r=a$. In the case of Ψ_f^-, at least one channel is open and the corresponding continuum wave function satisfies the standard open channel asymptotic boundary condition for Coulomb waves. For Ψ_i, all channels are closed and the continuum functions all decay exponentially as $r \to \infty$.

The R-matrix method is extended to double photoionization by employing the RMPS method [4], in which the continuum associated with the N-electron ion is represented by a set of pseudo-orbitals. We employ nonorthogonal Laguerre pseudo-orbitals of the form

$$P_{\bar{n}l}(r) = N_{\bar{n}l}(\lambda_{\bar{n}l}zr)^{l+1}e^{-\lambda_{\bar{n}l}zr/2}L_{\bar{n}+l}^{2l+1}(\lambda_{\bar{n}l}zr). \tag{4}$$

Here, $z=Z-N+1$, where Z is the nuclear charge; $L_{\bar{n}+l}^{2l+1}$ is the associated Laguerre polynomial; and $N_{\bar{n}l}$ is a normalization constant. We then orthogonalize these orbitals to each other and the spectroscopic orbitals. The scaling parameters $\lambda_{\bar{n}l}$ can be used to adjust the energy and the radial extent of the pseudostates. We employ a method developed by Gorczyca and Badnell [4] to orthogonalize the $(N+1)$-electron continuum basis orbitals to the Laguerre pseudo-orbitals. The double photoionization cross section is then calculated as the sum of all cross sections for single photoionization with excitation to those pseudostates that are above the ionization limit of the N-electron ion.

For all our RMPS calculations of the double photoionization of Ne, we employed the program AUTOSTRUCTURE [28] to determine Thomas-Fermi-Dirac-Amaldi spectroscopic orbitals for the $1s$-$4f$ subshells. In order to represent the high-Rydberg states and continuum of the singly ionized species, we then used the same program to generate the Laguerre pseudo-orbitals $\bar{n}l$ from $\bar{n}=5$ to some upper limit and $l=0$–4.

For our first calculation of the double photoionization of Ne, the target expansion for Ne^+ included the terms arising from the spectroscopic configurations $2s^22p^5$, $2s2p^6$, $2s^22p^4nl$, and $2s2p^5nl$ with nl from $3s$ to $4f$, along with the pseudostate configurations $2s^22p^4\bar{n}l$ and $2s2p^5\bar{n}l$ with $\bar{n}=5$–12 and $l=0$–4. In the case of the $2s2p^5nl$ spectroscopic configurations, all terms are well above the first ionization limit of Ne^+ and are, therefore, autoionizing. This basis leads to a total of 829 terms in both the CI and the CC expansions. We refer to this calculation as model 1.

Ideally, in order to determine whether a given calculation is converged with respect to the pseudostate expansion, one would add additional layers of $2s^22p^4\bar{n}l$ and $2s2p^5\bar{n}l$ pseudostates and compare the resulting double photoionization cross section with that from the smaller calculation. However, since the $2s2p^5\bar{n}l$ pseudostates are significantly higher in energy than those from the $2s^22p^4\bar{n}l$ configurations, for

our next set of calculations we kept the maximum value of $\bar{n}$ for the $2s2p^5\bar{n}l$ pseudostates fixed at 12 and added additional $2s^22p^4\bar{n}l$ pseudostates. We first increased the maximum value of $\bar{n}$ for the $2s^22p^4\bar{n}l$ pseudostates to 13, resulting in 879 terms (model 2); and finally to 14, resulting in 929 terms (model 3). The size of the R-matrix box, the number of basis orbitals used to represent the continuum wave functions in the inner region, and the number of pseudostates above the first ionization limit of Ne^+ changed somewhat with these three models. The radius of the R-matrix box varied from 37.2 a.u. for model 1 to 41.6 a.u for model 3; 45 basis orbitals provided an adequate representation of the continuum for model 1, but had to be increased to 50 for model 3; and for model 1, 732 out of the 829 terms were above the ionization limit of Ne^+, while for model 3, 825 out of the 929 terms were above this ionization limit.

At first, it may appear that one could achieve more complete pseudostate convergence by separating the RMPS calculation for the $2s^22p^4nl$ series from that for the $2s2p^5nl$ series. However, since the interaction between these two series should be quite strong, such a separation could lead to inaccurate results. Indeed, two separate test calculations of double photoionization to $2s^22p^4$ and $2s2p^5$ confirmed this. The first one that included only $2s^22p^5$, $2s^22p^43l$, $2s^22p^44l$, and the $2s^22p^4\bar{n}l$ pseudostates from $\bar{n}=5$ to 12 and from $l=0$ to 4 yielded a double photoionization cross section that was relatively free of pseudoresonances and was about 30% below that from model 1, described above. The second one that used an expansion that included only $2s^22p^5$, $2s2p^6$, $2s2p^53l$, $2s2p^54l$, and the $2s2p^5\bar{n}l$ pseudostates from $\bar{n}=5$ to 12 and from $l=0$ to 4 yielded a cross section with a background of about 35% of the cross section from model 1; however, it also displayed a very large resonance structure that is completely unphysical.

All the RMPS scattering calculations for the inner region were performed using significantly modified parallel versions [29] of the RMATRX I suite of codes [30,31]. These programs generate the surface amplitudes, the R-matrix poles, the $(N+1)$-electron eigenvectors, and the dipole matrices needed to determine the photoionization cross sections. A modified version of the program STGB was used to determine the initial bound states of the $(N+1)$-electron atom and a parallel program derived from the serial code STGBF was employed to do all calculations in the outer region and generate the photoionization cross sections as a function of energy.

III. RESULTS

The calculated energies for Ne^+ in comparison to experimental values for the lowest 21 terms of the 929 terms included in the RMPS calculation from model 3 are given in Table II. The energy levels from the other two models are very close to those given in this table. The average difference between the experimental and the theoretical energies is 2.9%. The calculated ionization energy from the $2s^22p^6\ ^1S$ ground term of Ne is 1.842 Ry, compared to the experimental value of 1.585 Ry; this difference of 0.257 Ry amounts to a 16% error. As discussed in Sec. I, this relatively large error arises from the fact the $(N+1)$-electron bound states for neutral Ne are highly correlated, while those for Ne^+ include much less correlation.

TABLE II. Energies of the first 21 terms in Ne^+ relative to the ground term.

No.	Term	Expt. energy[a] (Ry)	Theor. energy[b] (Ry)	% Diff.[c]
1	$2s^22p^5\ ^2P$	0.0000	0.0000	
2	$2s2p^6\ ^2S$	1.9779	1.9913	0.7
3	$2s^22p^4(^3P)3s\ ^4P$	1.9968	2.0537	2.8
4	$2s^22p^4(^3P)3s\ ^2P$	2.0439	2.1144	3.3
5	$2s^22p^4(^3P)3p\ ^4P$	2.2448	2.3048	2.6
6	$2s^22p^4(^1D)3s\ ^2D$	2.4532	2.3293	5.3
7	$2s^22p^4(^3P)3p\ ^4D$	2.2727	2.3344	2.6
8	$2s^22p^4(^3P)3p\ ^2D$	2.2892	2.3512	2.6
9	$2s^22p^4(^3P)3p\ ^2S$	2.3037	2.3681	2.7
10	$2s^22p^4(^3P)3p\ ^4S$	2.3051	2.3681	2.7
11	$2s^22p^4(^3P)3p\ ^2P$	2.3165	2.3843	2.8
12	$2s^22p^4(^1D)3p\ ^2F$	2.5004	2.5846	3.3
13	$2s^22p^4(^1D)3p\ ^2P$	2.5183	2.6007	3.2
14	$2s^22p^4(^1S)3s\ ^2S$	2.5213	2.7060	6.8
15	$2s^22p^4(^1D)3p\ ^2D$	2.5273	2.6127	3.3
16	$2s^22p^4(^3P)3d\ ^4D$	2.5445	2.6055	2.3
17	$2s^22p^4(^3P)3d\ ^2D$	2.5547	2.6179	2.4
18	$2s^22p^4(^3P)3d\ ^4F$	2.5567	2.6172	2.3
19	$2s^22p^4(^3P)3d\ ^2F$	2.5569	2.6199	2.4
20	$2s^22p^4(^3P)3d\ ^4P$	2.5611	2.6215	2.3
21	$2s^22p^4(^3P)3d\ ^2P$	2.5660	2.6270	2.3

[a]NIST atomic spectroscopic data [32].
[b]From the present 929-term CI calculation (model 3).
[c]The average is 2.9%.

The double photoionization cross sections from the ground term of Ne from models 1–3, in both the length and the velocity gauges, are shown in Fig. 1. They are determined from the cross section for single photoionization with excitation to all pseudostate terms above the experimental ionization energy of Ne^+. The threshold for double photoionization was then adjusted to the experimental value by adjusting the theoretical value for the ionization limit of Ne to the experimental value. These curves display the size of the pseudoresonances as a function of the number of $2s^22p^4\bar{n}l$ pseudostates included in the CC expansion. One would expect the pseudoresonances attached to the pseudostates included in the CC expansion to decrease in magnitude as the pseudostate basis is increased. As can be seen, this does occur gradually as we move from model 1 to model 3, especially for the cross sections calculated in the velocity gauge.

To provide clearer comparisons of the results from these three calculations, we made fourth-order polynomial fits to the raw cross-section data shown in Fig. 1, and these fits are shown in Fig. 2. As can be seen, the cross sections calculated in the velocity gauge from model 1 to model 3 are extremely close, indicating a good convergence. The length-gauge cross

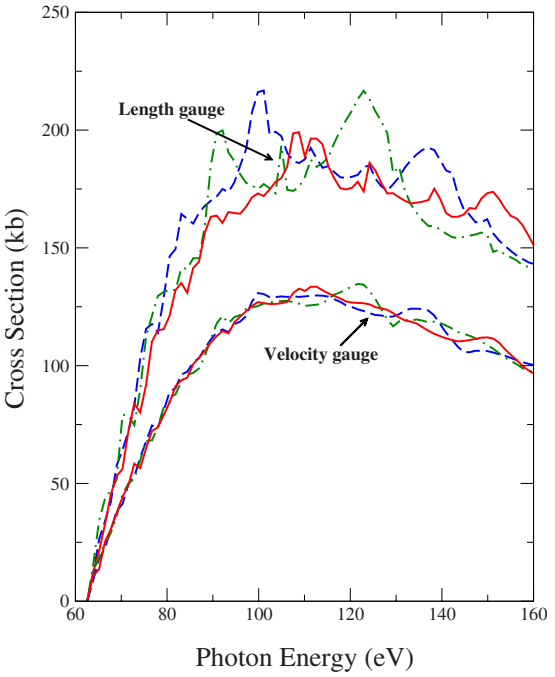

FIG. 1. (Color online) Ne double photoionization cross sections from the present length-gauge and velocity-gauge RMPS calculations, showing the size of the pseudoresonances. The dotted-dashed curves are from the 829-term RMPS calculation (model 1), the dashed curves are from the 879-term RMPS calculation (model 2), and the solid curves are from the 929-term RMPS calculation (model 3) (1.0 kb=1.0×10^{-21} cm^2).

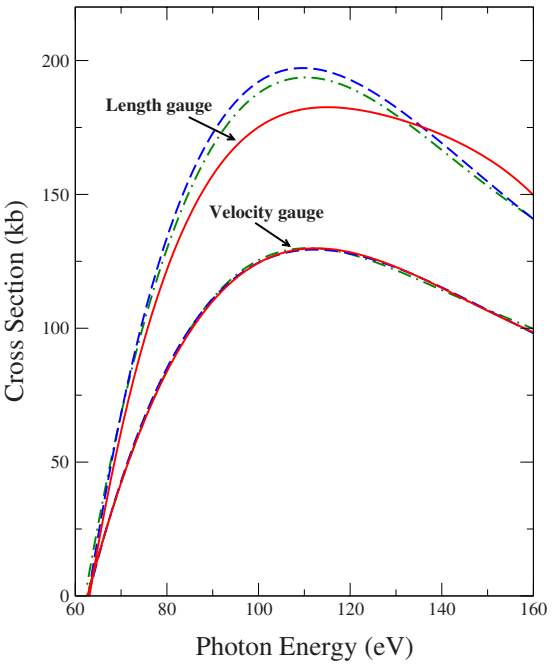

FIG. 2. (Color online) Ne double photoionization cross sections determined from polynomial fits to the present length- and velocity-gauge RMPS calculations. The dotted-dashed curves are from the 829-term RMPS calculation (model 1), the dashed curves are from the 879-term RMPS calculation (model 2), and the solid curves are from the 929-term RMPS calculation (model 3) (1.0 kb=1.0 $\times10^{-21}$ cm^2).

section increases slightly in going from model 1 to model 2; and, at the peak, it decreases in magnitude by about 6% from model 2 to model 3. The fit to model 3 in the length gauge is above the fits to models 1 and 2 at photon energies above 133 eV, at least partially because of the pseudoresonances in model 3 within this energy range. At the cross-section peaks, the ratio of the velocity-gauge to the length-gauge cross sections is 0.67 and 0.66 for models 1 and 2, respectively, but has increased to 0.71 for model 3. These ratios are significantly lower than those that we obtained in our work on Be and Mg [13]; however, this is not surprising in light of the imbalance between the correlations included in the initial and the final states, as discussed in Sec. I.

In Fig. 3, we compare the polynomial fits to both the present length-gauge and velocity-gauge cross sections from model 3 with both MBPT results and experimental cross sections obtained from a variety of synchrotron measurements. The measurements of Samson and Angel [24] and those of Holland *et al.* [23] vary by as much as 100 kb, making comparisons of experiment with theory difficult. The length-

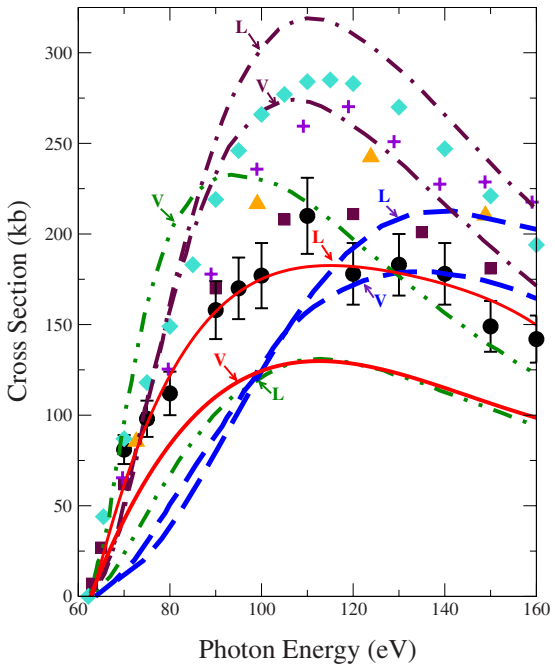

FIG. 3. (Color online) Double photoionization cross section of Ne. The solid curves are from the polynomial fits to the present length-gauge (L) and velocity-gauge (V) 929-term RMPS calculations (model 3). The dashed-double-dotted and the dashed-dotted curves are from the length (L) and the velocity (V) MBPT calculations of Kilin *et al.* [17] using the V^{N-2} and V^{N-1} Hartree-Fock potentials, respectively. The dashed curves are from the length (L) and the velocity (V) MBPT calculations of Carter and Kelly [16] using a V^{N-1} Hartree-Fock potential. The solid diamonds are from the measurements of Samson and Angel [24], the plus signs are from the measurements of Wight and Van der Wiel [22], the solid triangles are from the measurements of Schmidt *et al.* [21], the solid squares are from the experimental measurements of Bartlett *et al.* [25], and the solid circles are from the measurements of Holland *et al.* [23] (1.0 kb=1.0×10^{-21} cm^2).

gauge cross section determined from model 3 is in excellent agreement with the measurements of Holland *et al.*, but low compared to all other experimental results, while the velocity-gauge cross section is low compared to all experimental measurements. The length-gauge MBPT cross section from Carter and Kelly [16], in which their basis wave functions were calculated in the potential of Ne^+ (V^{N-1}), has a peak magnitude that is close to the experimental results of Bartlett *et al.* [25]. However, their velocity gauge results are about 16% lower and the peaks in their MBPT cross sections are at higher energies than any of the experimental cross sections. We also show two length-gauge and two velocity-gauge MBPT cross sections from Kilin *et al.* [17]. The V^{N-1} potential length-gauge result is approximately 2.4 times higher than the V^{N-2} length-gauge cross section, and the ratio of the velocity-gauge to the length-gauge cross section is 0.86 for the V^{N-1} potential and 1.75 for the V^{N-2} potential. When Kilin *et al.* [18] used a V^{N-q} potential and varied the fractional charge q to minimize the difference between the length-gauge and the velocity-gauge cross sections, they obtained a result close to their V^{N-1} potential velocity-gauge cross section shown in Fig. 3. However, it is quite surprising that the V^{N-1} results of Kilin *et al.* [17] vary so much from those of Carter and Kelly [16].

IV. SUMMARY

We have completed a series of R matrix with pseudostate calculations of total double photoionization from the ground term of Ne. These RMPS calculations were performed in both the length and the velocity gauges and the length and the velocity results are not nearly as close as they were for our earlier calculations of double photoionization in Be and Mg [13]. However, this should be expected on the basis of the complexity of the configurations remaining after double photoionization of Ne compared to the closed-shell configurations remaining after double photoionization of Be and Mg. Within the limits of currently available massively parallel computers, we were able to achieve a reasonably converged result, especially in the velocity gauge. However, due to large variations between the results of various synchrotron measurements, it is difficult to draw any definitive conclusions regarding the accuracy of the present results.

ACKNOWLEDGMENTS

This work was supported in part by grants from the U.S. Department of Energy. The computational work was carried out at the National Energy Research Scientific Computing Center in Oakland, California.

[1] J. Z. Tang and I. Shimamura, Phys. Rev. A **52**, R3413 (1995).
[2] A. S. Kheifets and I. Bray, Phys. Rev. A **54**, R995 (1996).
[3] K. W. Meyer, C. H. Greene, and B. D. Esry, Phys. Rev. Lett. **78**, 4902 (1997).
[4] T. W. Gorczyca and N. R. Badnell, J. Phys. B **30**, 3897 (1997).
[5] M. S. Pindzola and F. Robicheaux, Phys. Rev. A **57**, 318 (1998).
[6] M. S. Pindzola and F. Robicheaux, Phys. Rev. A **58**, 779 (1998).
[7] J. Colgan and M. S. Pindzola, Phys. Rev. A **65**, 032729 (2002).
[8] J. Colgan and M. S. Pindzola, Phys. Rev. A **67**, 012711 (2003).
[9] A. S. Kheifets and I. Bray, Phys. Rev. A **65**, 012710 (2001).
[10] J. Colgan and M. S. Pindzola, Phys. Rev. A **65**, 022709 (2002).
[11] F. Citrini, L. Malegat, P. Selles, and A. K. Kazansky, Phys. Rev. A **67**, 042709 (2003).
[12] A. S. Kheifets and I. Bray, Phys. Rev. A **75**, 042703 (2007).
[13] D. C. Griffin, M. S. Pindzola, C. P. Ballance, and J. Colgan, Phys. Rev. A **79**, 023413 (2009).
[14] T. N. Chang, T. Ishihara, and R. T. Poe, Phys. Rev. Lett. **27**, 838 (1971).
[15] T. N. Chang and R. T. Poe, Phys. Rev. A **12**, 1432 (1975).
[16] S. L. Carter and H. P. Kelly, Phys. Rev. A **16**, 1525 (1977).
[17] V. A. Kilin, D. A. Lazarev, Dm. A. Lazarev, M. Y. Amusia, K.-H. Schartner, A. Ehresmann, and H. Schmoranzer, J. Phys. B **33**, 4989 (2000).
[18] V. A. Kilin, D. A. Lazarev, Dm. A. Lazarev, V. M. Zelichenko, M. Y. Amusia, K.-H. Schartner, A. Ehresmann, and H. Schmoranzer, J. Phys. B **34**, 3993 (2001).
[19] T. A. Carlson, Phys. Rev. **156**, 142 (1967).
[20] J. A. R. Samson and G. N. Haddad, Phys. Rev. Lett. **33**, 875 (1974).
[21] V. Schmidt, N. Sander, H. Kuntzemuller, P. Dhez, F. Wuilleumier, and E. Kallne, Phys. Rev. A **13**, 1748 (1976).
[22] G. R. Wight and M. J. Van der Wiel, J. Phys. B **9**, 1319 (1976).
[23] D. M. P. Holland, K. Codling, G. V. Marr, and J. B. West, J. Phys. B **12**, 2465 (1979).
[24] J. A. R. Samson and G. C. Angel, Phys. Rev. A **42**, 5328 (1990).
[25] R. J. Bartlett, P. J. Walsh, Z. X. He, Y. Chung, E. M. Lee, and J. A. R. Samson, Phys. Rev. A **46**, 5574 (1992).
[26] P. G. Burke and K. T. Taylor, J. Phys. B **8**, 2620 (1975).
[27] K. A. Berrington, P. G. Burke, K. Butler, M. J. Seaton, P. J. Storey, K. T. Taylor, and Y. Yan, J. Phys. B **20** 6379 (1987).
[28] N. R. Badnell, J. Phys. B **30**, 1 (1997).
[29] C. P. Ballance and D. C. Griffin, J. Phys. B **39**, 3617 (2006).
[30] N. J. Scott and P. G. Burke, J. Phys. B **13**, 4299 (1980).
[31] K. A. Berrington, W. B. Eissner, and P. H. Norrington, Comput. Phys. Commun. **92**, 290 (1995).
[32] http://physics.nist.gov/PhysRefData/contents-atomic.html